ACTA IMEKO
ISSN: 2221-870X
March 2022**, Volume **11**, Number **1**, 1 - **10

Decay of a Roman age pine wood studied by micro magnetic resonance imaging, diffusion nuclear magnetic resonance and portable nuclear magnetic resonance

Valeria Stagno[1,2], Silvia Capuani[2,3]

[1] *Earth Sciences Department, Sapienza University of Rome, Piazzale Aldo Moro 5, 00185 Rome, Italy*
[2] *National Research Council - Institute for Complex Systems (CNR-ISC) c/o Physics Department Sapienza University of Rome, Piazzale Aldo Moro 5, 00185 Rome, Italy*
[3] *Centro Fermi - Museo Storico Della Fisica e Centro Studi e Ricerche Enrico Fermi, Piazza del Viminale 1, Rome 00184, Italy*

ABSTRACT
Wood is a hygroscopic biodegradable porous material widely used by men in the past to create artworks. Its total preservation over time is quite rare and one of the best preservation modalities is waterlogging. Observing the anatomy of waterlogged archaeological wood could also be complicated because of its bacterial degradation. However, the characterization of wood morphology and conservation state is a fundamental step before starting any restoration intervention as it allows to extract information about past climatic conditions and human activities. In this work, a micro-invasive approach based on the combined use of high-resolution magnetic resonance imaging (MRI) and diffusion-nuclear magnetic resonance (NMR) was tested both on a modern and an ancient pine wood sample. Furthermore, a completely non-invasive analysis was performed by using portable NMR. This multi-analytical NMR approach allowed to highlight the effect of decay on the wood microstructure, through alterations in the pores size, tortuosity, and images contrast of the ancient pine compared to the modern one. This work pointed out the different but complementary multi-parametric information that can be obtained by using NMR and tested the potential of high-field MRI and low-field portable NMR in the detection of wood diagnostic features..

Section: RESEARCH PAPER

Keywords: Archaeological waterlogged wood; micro-MRI; diffusion-NMR; portable NMR

Citation: Valeria Stagno, Silvia Capuani, Decay of a Roman age pine wood studied by micro magnetic resonance imaging, diffusion nuclear magnetic resonance and portable nuclear magnetic resonance, Acta IMEKO, vol. 11, no. 1, article 12, March 2022, identifier: IMEKO-ACTA-11 (2022)-01-12

Section Editor: Fabio Santaniello, University of Trento, Italy

Received March 3, 2021; **In final form** March 15, 2022; **Published** March 2022

Corresponding author: Valeria Stagno, e-mail: valeria.stagno@uniroma1.it

1. INTRODUCTION

Wood is a porous material with complex morphology. In the past, it has been widely used by men to produce artworks. For this reason, wood is widespread in the cultural heritage world and its microstructure has always been studied for the species identification, for dendrochronological analyses and for extracting important information about ancient human activities [1]. Two principal types of wood can be recognized: softwood and hardwood. Softwood has a very homogeneous structure mainly composed of tracheids and fibre-tracheids [2]. The resin canals are one of its main characteristics that allow it to be distinguished from the hardwood. In addition, its annual rings are usually well separated through the annual ring limit and they are made of an earlywood area, with pores characterized by larger lumens and thinner walls, and a latewood area with thicker walls and smaller lumens [2]. However, these two areas are not always well differentiated. Some softwoods present an abrupt passage from earlywood to latewood, while some others a gradual one [2]. Among the many anatomical elements described above, the growth ring is surely one of the most important because its characterization provides the age of the tree and the climatic conditions in which it has grown [3], [4], as well as being crucial for the species identification. Because of its biodegradability [4] wood is hardly preserved with no microstructural alterations. Waterlogged wood is usually well preserved for the microscopic observation of its annual rings, especially when the wooden object was buried under the sea sediments [6]. In fact, thanks to the anaerobic conditions fungal attacks are more or less excluded

[6] and if the object was buried under the seabed also the marine borer activity is limited [7]. In this environment, the main degradation can be attributed to erosion bacteria [8]-[10]. Conversely, at a macroscopic level the wood rings are not always visible with the naked eye because of changes in colour, consistency, and superficial morphology of the wood structure [11]. As a consequence, microscopic imaging techniques are always required. Moreover, the evaluation of the effect of age is also very important, for example, to determine the conservation state of an artwork. Knowing the state of wooden remains, such as its degree of decay and its pore size and morphology, is useful for planning the restoration and choosing the restoration materials [11], [12]. In the literature, several works [13]-[22] about the use of nuclear magnetic resonance (NMR) on wooden artworks have proven its utility in the microstructural characterization and the evaluation of their conservation state. The above cited works employed invasive or destructive NMR techniques, while some others [22]-[25] pointed out the potential of non-invasive portable NMR. Among these, our previous work Stagno et al. [23] showed how 1D and 2D low-field NMR experiments can be used as complementary techniques to study water compartmentalization in archaeological waterlogged wood with the support of optical microscopy and magnetic resonance images. Furthermore, we suggested the ability of low-field NMR in detecting cell wall decay and paramagnetic impurities. In respect to our previous work [23], in this study we investigated a decayed pine wood of the Roman age by using MR images with higher resolution and by characterizing the wood structure also with the pore size distribution extracted from the relaxation measurements. The results obtained from the archaeological sample were compared with the results obtained from its modern counterpart. Specifically, the aim of this work was to test the potential of NMR multi-analytical approach to evaluate archaeological wood decay. We compared micro-invasive magnetic resonance imaging (MRI) and diffusion-NMR [26]-[29] with non-invasive portable NMR [30], [31]. The potential of MR images as an alternative approach to the conventional techniques for the characterization of the annual rings, as well as of all the diagnostic features of waterlogged wood, was tested. Moreover, high-field diffusion and low-field portable NMR were used to highlight the effect of decay on the wood microstructure, such as variations in the pore size of the ancient compared to the modern pine.

2. BACKGROUND THEORY

2.1. Diffusion-NMR and pore size

Molecules constituting a fluid whose absolute temperature is greater than zero Kelvin are in constant movement because of their kinetic energy [27]. This process is called self-diffusion. When a fluid totally fills porous medium, molecules moving with random motion are subject to continuities deviations of their trajectories due to collision with the pores walls. Diffusion-NMR techniques investigate diffusion dynamics by following in time the fluid molecules. The root mean square distance travelled, ℓ_D (or diffusion length), increases with time as long as no boundaries are encountered, according to the Einstein relation: $\ell_D = \sqrt{2\,n\,D\,t}$ where $n = 1, 2, 3$ is the space dimension and D is the bulk diffusion coefficient that can be measured by a Pulsed Field Gradient sequence [26]. At a fixed diffusion time $t = \Delta$ (where Δ is the delay time between the two gradient pulses) and fixed pulse magnetic-field gradient duration δ such that $\delta \ll \Delta$, it is possible to vary the magnetic-field gradient strength g, so that the NMR-signal amplitude $S(g)$ is given by [28], [32]:

$$S(g) = S(0)\, \mathrm{e}^{-\gamma^2 g^2 \delta^2 D\left(\Delta - \frac{\delta}{3}\right)}, \tag{1}$$

where γ is the gyromagnetic ratio of protons, $b =$ is the so called b-value, D is the diffusion coefficient obtained at a specific diffusion time Δ and $S(0)$ is the signal at g =0. Since during Δ in a Pulsed Gradient Stimulated Echo (PGSTE) experiment longitudinal relaxation decay T_1 would occur, the maximum Δ accessible is limited by the relation $\Delta < T_1$ [33]. Geometrical restrictions of the medium, such as the pores walls, lead to a $D(\Delta)$ decreasing with time. In a heterogeneous porous system as wood, it is possible to derive useful information about pores size, pores interconnection and membrane permeability [29] by studying the $D(\Delta)$ behaviour.

In the case of long Δ limit (i.e., $\Delta \gg L^2/D_0$, where L is the mean pore diameter) and impermeable wall, the water diffusion coefficient varies according to:

$$D(\Delta) = \frac{L^2}{2\,\Delta}. \tag{2}$$

Equation (2) indicates that L can be obtained from the slope of D vs Δ^{-1}. However, deviation from equation (2) can occur for semi-permeable walls [34]-[35]. For materials with interconnected pores, at very long times $D(\Delta)$ approaches an asymptotic value D_∞ that is independent of the diffusion time Δ and directly related to the tortuosity τ of the porous material:

$$\tau = \frac{D_0}{D_\infty}. \tag{3}$$

Tortuosity is an intrinsic property of a porous medium usually defined as the ratio of actual flow path length to the straight distance between the ends of the flow path. So, τ of the porous system reflects the connectivity degree of the porous network [36]-[38].

2.2. Transversal relaxation and pore size

The transversal or spin-spin relaxation time T_2 is due to the loss of coherence of the spins among themselves. When an ensemble of spins is considered, their magnetic fields interact (spin-spin interaction), slightly modifying their precession rate. These interactions are temporary and random. Thus, spin-spin relaxation causes a cumulative loss in phase resulting in transverse magnetization decay [26]. In a porous medium, the T_2 relaxation of the fluid (e.g., water) is given by the sum of different contributions [39]-[43]:

$$\frac{1}{T_2} = \frac{1}{T_{2\mathrm{b}}} + \frac{1}{T_{2\mathrm{s}}} + \frac{D(\gamma\, G\, T_\mathrm{E})^2}{12}, \tag{4}$$

where $1/T_2$ is the total spin-spin relaxation rate, $1/T_{2\mathrm{b}}$ is the relaxation rate of bulk water and $1/T_{2\mathrm{s}}$ is the relaxation rate of water on the pore surface. The term $D(\gamma\, G\, T_\mathrm{E})^2/12$ is related to the dephasing caused by the presence of a magnetic field gradient G, named "diffusion relaxation" term. D is the diffusion coefficient of water in the porous system, γ is the hydrogen gyromagnetic ratio and T_E is the echo time.

When the T_2 is measured by a Carr-Purcell Meiboom-Gill (CPMG) sequence, the contribution of diffusion relaxation is averaged out by means of an echo train if a very short T_E is selected [44], [45]. In the presence of a porous system, the

dominant relaxation rate is $1/T_{2s}$ while the term $1/T_{2b}$ can be neglected because of the low efficiency of bulk water relaxation [46]. Equation (4) becomes:

$$\frac{1}{T_2} \approx \frac{1}{T_{2s}} = \rho \frac{S}{V}, \tag{5}$$

where ρ is the surface relaxivity [46], S/V is the surface-to-volume ratio of the pore. Therefore, by measuring the spin-spin relaxation in a porous medium the pore diameter d can be calculated by [46]-[48]:

$$\frac{1}{T_2} = \rho \frac{2\,n}{d}, \tag{6}$$

where n is a shape factor (for our samples a spherical shape was considered, $n = 3$).

3. MATERIALS AND METHODS

3.1. Samples

Two cylinders-like wood samples of a water-soaked modern wood and an archaeological waterlogged wood were studied. Their size was less than 15 mm in length and 8 mm in diameter, suitable for a 10 mm NMR tube. The archaeological sample detached from an ancient pole of the Roman harbour of Naples, dated to the V century AD [49], [50]. It was well preserved in waterlogged conditions and for this reason was always kept in water during the analysis. The modern wood, instead, was previously maintained at the environmental conditions of 20 °C and 50 % of relative humidity. In order to perform NMR acquisitions, the modern sample was imbibed with distilled water until the saturation was reached. Both the species of modern and archaeological wood was stone pine (*Pinus pinea* L.) [51], [52].

3.2. High-field NMR acquisitions

All the high-field NMR analyses were performed by using a 400 MHz Bruker-Avance spectrometer with a 9.4 T static magnetic field and a micro-imaging unit equipped with high-performance and high-strength magnetic field gradients for MRI and diffusion measurements. The gradients maximum strength was 1240 mT/m and the rise time 100 μs.

To measure the diffusion coefficient D and the longitudinal relaxation time T_1, useful to choose the longest observation time Δ accessible during the diffusion experiments according to the $\Delta < T_1$ relation, the soaked samples were inserted without additional water in the NMR tube, which was sealed on the top with Parafilm in order to prevent the sample dehydration. The longitudinal relaxation time was measured with a Saturation-Recovery S_R sequence with 128 points from 10 μs to 10 s, repetition time T_R of 10 s, number of scans N_S equal to 4. The acquisition time was 1 hour and 40 minutes for each sample. For the measurement of the water diffusion coefficient, a PGSTE sequence [28], [29] was used. The diffusion was evaluated along the x axis (i.e., perpendicular to the main direction of the wood grain) corresponding to the radial direction. The PGSTE signal was obtained using $T_R = 5$ s, echo time $T_E = 1.9$ ms, pulse gradient duration $\delta = 3$ ms, 32 steps of the gradient strength g, from 26 to 1210 mT/m, for each diffusion time Δ and $N_S = 16$. The Δ values used were 0.04 - 0.08 - 0.12 - 0.16 - 0.2 - 0.3 - 0.4 s. The b-value spanned from a minimum of 1.6×10^7 s/m² to a maximum of 9.5×10^{11} s/m². The acquisition time was about 6 hours for each sample.

Table 1. Acquisition parameters of T_2*-weighted images.

Parameters	Modern pine	Archaeological pine
T_E/T_R (ms)	3/1200	5/1500
Number of Slice	3	3
N_S	128	128
STK (μm)	200	300
FOV (cm²)	0.9 × 0.9 / 1.4 × 1.4	0.9 × 0.9
MTX (pixels)	512 × 512	512 × 512
R (μm²)	18 × 18 / 27 × 27	18 × 18

For the acquisition of MR images, the samples were inserted with distilled water in the NMR tube and sealed with Parafilm in order to prevent water evaporation. In this way, T_2^*-weighted images were performed with a Gradient Echo Fast Imaging (GEFI) sequence [26] in the transversal, tangential and radial direction. The images were weighted on the T_2^* parameter, which depends on both T_2 and magnetic field inhomogeneities. The optimized parameters used in the GEFI sequence are reported in Table 1, where *STK* is the slice thickness, *FOV* the field of view, *MTX* the image matrix and *R* the in-plane resolution.

3.3. Low-field portable NMR acquisitions

For the low-field NMR acquisitions the samples were just placed on the surface of the sensitive area of the portable spectrometer. A Bruker minispec mq-ProFiler with a single-sided magnet that generates a static magnetic field of 0.35 T with a ^{1}H resonance frequency of 15 MHz and dead time of 2 μs was used. The single-sided NMR was equipped with a RF coil for performing experiments within 2 mm starting from the sample surface to the inside of the sample [53].

The portable spectrometer has a constant magnetic gradient field with strength of about 3 T/m.

The transversal relaxation time T_2 was measured with a CPMG sequence with $T_E = 42$ μs, 6500 echo times, $T_R = 1$ s, $N_S = 128$ and acquisition time of about 5 minutes.

3.4. Data processing

The longitudinal relaxation time was obtained by plotting the signal intensities S as a function of $t = S_R$ delays for fitting the following equation:

$$S(t) = M\left[1 - \mathrm{e}^{-\frac{t}{T_1}}\right] \tag{7}$$

to data, where T_1 is the longitudinal relaxation time and M is the associated equilibrium magnetization.

The diffusion coefficient values were obtained by fitting the following equation:

$$S(b) = M_1\,\mathrm{e}^{-D_1 b} + M_2\,\mathrm{e}^{-D_2 b} \tag{8}$$

to data acquired at different b-values, where $S(b)$ is the NMR signal as function of the b-value, D_1 and D_2 are the two components of the diffusion coefficient associated with the magnetizations M_1 and M_2, respectively. The fit goodness was evaluated by the $\overline{R^2}$ (i.e., the R^2 corrected for the number of the regressors). Fits of equation (7) and equation (8) were performed by using the OriginPro 8.5 software.

Plots of the diffusion coefficient D vs. the diffusion time Δ were performed with MatlabR2019b. From the D vs. Δ trend, the first and last points, corresponding to the free water diffusion and the diffusion through semi-permeable membranes (i.e. the wood cell walls), were removed and the pores radius L was

estimated by the linear fit of equation (2) [54]. From the pores radius L, the pores diameter d was then calculated.

In addition, the value for $\Delta = \infty$ of the normalized diffusion coefficient $D(\Delta)/D_0$, where D_0 is the free water diffusion coefficient equal to 2.3 × 10^{-9} m^2/s, was calculated and used to evaluate tortuosity according to equation (3) [54]. Finally, the Inverse Laplace Transform [55] in Matlab (Matlab R2019b) was used to obtain the low-field T_2 distribution and the pores diameter distribution according to equation (6). The surface relaxivity ρ was previously estimated for the modern and ancient pine from the slope of the line given by T_2 time vs. pore size α, where α was calculated from diffusion measurements by the relation $\alpha = 2\sqrt{D\Delta}$ [46], [47].

4. RESULTS

T_2^*-weighted images of the transversal section of modern and archaeological stone pine are displayed in Figure 1a) and Figure 1b), respectively. Here, all the anatomical elements observable with conventional optical microscopy [51], [52] are detectable. First, the annual rings limit (white arrows) is well visible in both Figure 1a) and Figure 1b) with two separate areas with different contrast. In both modern and archaeological pine, the darker area corresponds to structures with low T_2^* values, while the brighter ones to structures with high T_2^* values [56]. These structures correspond to tracheids, which are considered as the predominant constituents of all softwoods [57]. The dark area is the latewood (light blue circles) while the bright area is the earlywood (green circles).

Resin canals (red circles), likely with the presence of resin, can also be observed. Moreover, rays (pink arrows) can be seen in both the samples but in Figure 1b) the archaeological pine shows black spots and artefacts (yellow circles) located along the rays and on the edge of the sample. These artefacts are typical of MR images of waterlogged woods [13] because of the deposition of impurities, i.e., bacterial erosion wood products and seabed sediments, in the wood microstructure during the burial period. These paramagnetic impurities provide a black contrast in T_2^*-images [58] revealing the distribution of the degradation zones since they are stored in the decayed structures of wood [13].

Figure 2a) and Figure 2b) display the radial section of modern and archaeological pine, respectively. In both the images, the anatomical element observable is the annual rings limit (white arrows) and in Figure 2b) the above-mentioned distribution of paramagnetic inclusions (yellow circles).

The tangential section of the modern and archaeological samples is shown in Figure 3a) and Figure 3b), respectively. The red circles highlight the tangential resin canals and the pink arrows the medullary rays. Again, in Figure 3b) the archaeological pine shows decayed zones (yellow circles) corresponding to black spots and artefacts produced by the presence of paramagnetic agents.

In Table 2 the relaxation time T_1 measured at high magnetic field and obtained by equation (7) is displayed. Both modern and archaeological pine show a T_1 around 500 ms. This limited the observation time Δ of the diffusion measurements, whose maximum value was set to 400 ms. In Figure 4a) and Figure 4b) the first (D_{x1}) and second (D_{x2}) diffusion component as function of the diffusion time Δ obtained by equation (8) are displayed.

In Table 3 the pores diameter and the tortuosity calculated from the high-field measurements by equation (2) and equation (3), respectively, are reported. In Figure 5a) the T_2 time distribution obtained by portable NMR is showed both for the modern (dashed line) and the ancient (solid line) pine. The pores size distribution calculated by equation (6) from the above mentioned low-field T_2-distribution is presented in Figure 5b) for the modern pine (dashed line) and the archaeological pine (solid line).

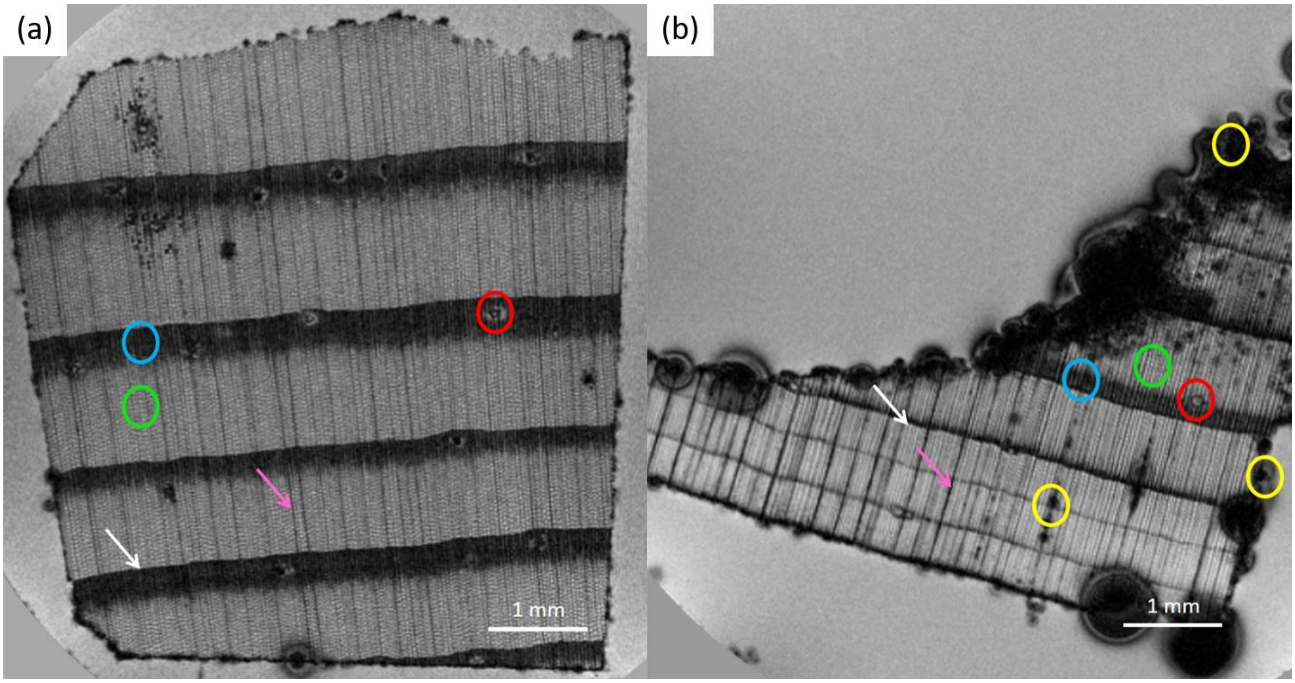

Figure 1. T_2*-weighted MR images of the transversal section of modern pine (a) and archaeological pine (b) obtained at high magnetic field (9.4 T). In both the samples there are resin canals (red circles), earlywood (green circles), latewood (blue circles), annual rings limit (white arrows) and rays (pink arrows). The ancient pine shows artefacts induced by paramagnetic ions in decayed areas (yellow circles).

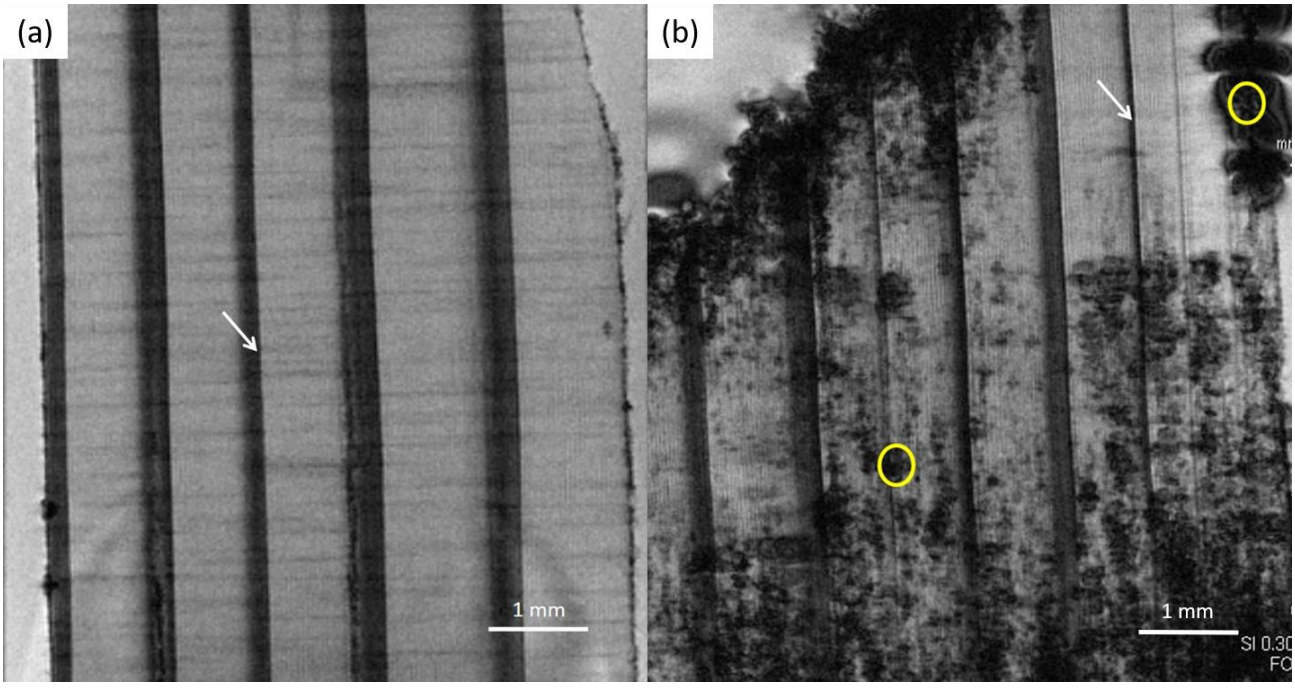

Figure 2. T_2*-weighted MR images of the radial section of modern pine (a) and archaeological pine (b) obtained at high magnetic field (9.4 T). In both the samples the annual rings limit (white arrows) is observable. The ancient pine shows artefacts induced by paramagnetic ions in decayed areas (yellow circles).

5. DISCUSSIONS

Compared to the conventional methods used to observe wood anatomy, i.e., optical microscopy or scanning electron microscopy, our MR images allowed to recognize some important diagnostic characters of wood especially in the transversal section (Figure 1).

Conversely, fewer characters were observed in the tangential (Figure 3) and radial (Figure 2) sections due to the current limitation on the resolution of MRI, whose maximum value is around 10 μm. Indeed, when the species of a softwood has to be recognized, the radial section is of fundamental importance because of its diagnostic features, such as pits of cross-fields and rays, which allow to discriminate among quite similar softwood structures (e.g., pine and spruce). However, the resolution of

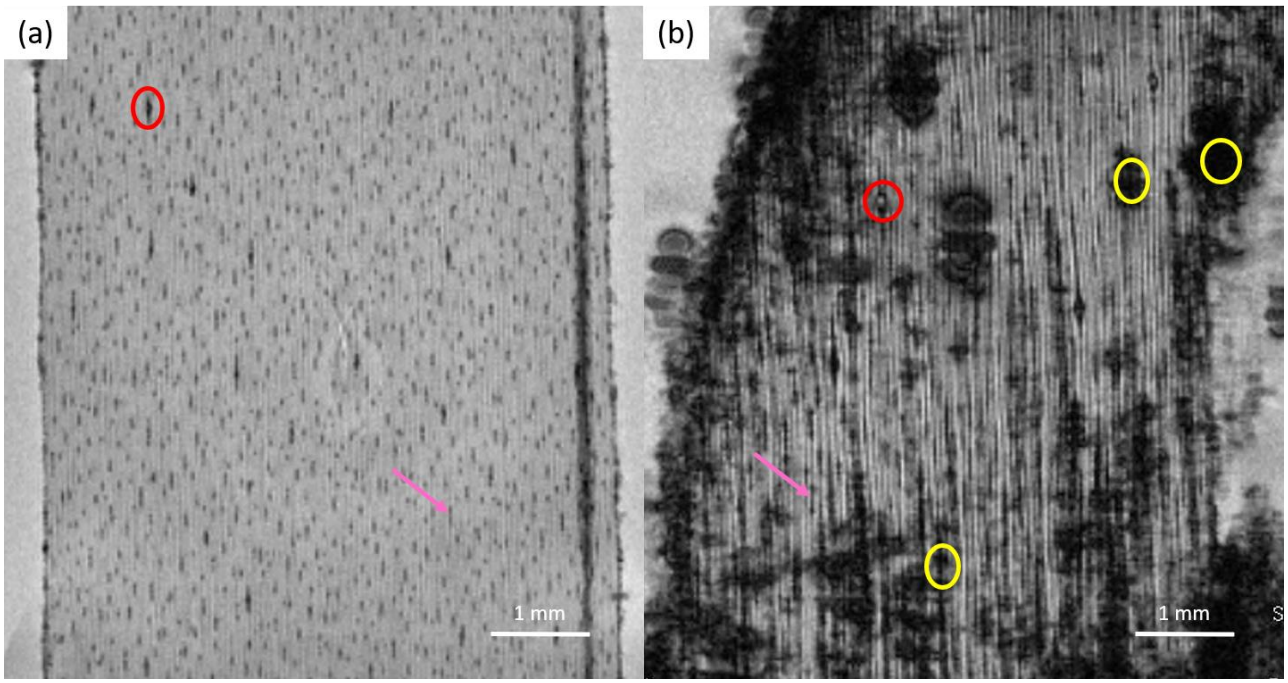

Figure 3. T_2*-weighted MR images of the tangential section of modern pine (a) and archaeological pine (b) obtained at high magnetic field (9.4 T). In both tangential resin canals (red circles) and rays (pink arrows) are observable. The ancient pine shows artefacts induced by paramagnetic ions in decayed areas (yellow circles).

Table 2. Longitudinal relaxation time T_1.

Sample	T_1 ± *SE* (ms)
Modern pine	541 ± 13
Archaeological pine	511 ± 19

MRI is not a physical limit but it depends on the characteristics of the instrumentation used.

In this work, MR images showed in Figure 1, Figure 2 and Figure 3 aim at investigating the decay effect and their specific contrast can be used to reconstruct the decay distribution and to detect the presence of paramagnetic impurities. All the sample volume can be imaged with MRI, whereas optical and scanning electron microscopy only provide images of a small portion of the wood sample. Moreover, the mechanical preparation of the sample in optical and scanning electron microscopy leads to its destruction if compared with the virtual sectioning operated by MRI. The longitudinal relaxation time T_1 could provide information about the water molecules surrounding environment, the sample structure and composition [26]. However, in a porous medium T_1 can be influenced by paramagnetic ions [59], [60] that usually cause its reduction, as found in Stagno et al. [23]. In our ancient wood many paramagnetic inclusions were detected as artifacts in the MR images [13] and T_1 values, displayed in Table 2, seem to be exchange averaged [59], therefore they do not include such detailed information about different structural compartments as T_2 value. For the aforementioned reason, the longitudinal relaxation time of our modern and ancient pine cannot be used to describe structural changes among them. Nevertheless, the measurement of T_1 is useful for setting the diffusion observation time. From the comparison of the transversal, radial and tangential section of the modern (Figure 1a, Figure 2a and Figure 3a) and the ancient (Figure 1b, Figure 2b and Figure 3b) pine, it is possible to observe morphological differences. First of all, the black spots (see section 4), can be associated with a degradation process operated by microorganisms with the inclusion of paramagnetic impurities (i.e., bacterial erosion wood products and burying sediments) into the wood structure. These black zones are not present in the modern wood and they are mostly located along the rays and on the edge of the sample (Figure 1b, Figure 2b and Figure 3b yellow circles). This indicates a strong degradation in these zones. The image contrast allows to observe that both the woods show well delimited growth rings. While the modern wood does not show particular changes in the annual ring thickness, in Figure 1b) the ancient pine has some thinner annual rings with no latewood. We can hypothesize that this is due to a climatic change during the tree growth (before the V century AD). In fact, thinner rings are usually attributed to not rainy periods [4], [11]. However, the ring thickness can be also influenced by other factors, for example the tree age. Therefore, more than one sample should be analysed to confirm our hypothesis.

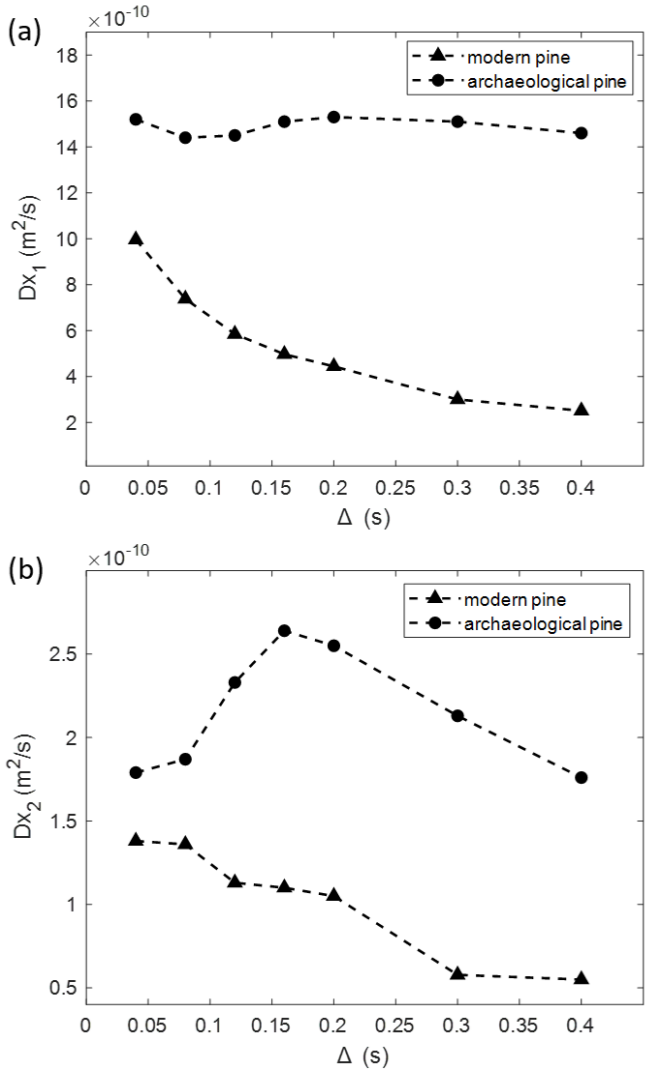

Figure 4. Plots (a) and (b) show the Dx_1 and Dx_2 decay as function of Δ for modern pine (circle markers) and archaeological pine (triangle markers). Dashed lines are for illustration purpose only.

The plots of the diffusion coefficient vs. the diffusion time in Figure 4a) and 4b) show that both wood samples have two main diffusion compartments but the diffusion in the modern pine is slower than in the ancient pine. The difference is around one order of magnitude for both the compartments D_{x1} and D_{x2}. This situation can be explained as the consequence of the degradation process that occurred in the ancient pine. In fact, the decay of the cellular structure and wood polymers may have produced the cell walls thinning and the lumens enlargement in the archaeological pine. From the point of view of a porous system, ancient pine is characterized by larger pores compared to modern pine. The existence of two different diffusion compartments means that both the woods have at least two main pores sizes as shown in Table 3. The two sizes d_1 and d_2 calculated from the high-field NMR diffusion measurements can be identified as the earlywood and latewood tracheids diameter [60], considering that tracheids are the main constituents of softwood. By comparing the calculated diameters of the modern and the ancient pine, despite in the earlywood the diameter seems to be similar between the two samples, for the latewood there is an increment of the tracheids size in the archaeological pine. A possible explanation is that the decay is higher in areas with high concentration of wood polymers, such as the latewood cell walls. These polymers are predominantly cellulose and hemicellulose that, as pointed out by high-resolution NMR spectra of both modern and ancient wood [19], are more degraded in respect to the usually well-preserved lignin. This result means that the greater the thickness of the cell wall, the stronger its deterioration. This is in agreement with the distribution of paramagnetic impurities revealed by the MR images, which follows the distribution of decay that is mainly located in rays

Table 3. Pores diameter, associated magnetizations and tortuosity obtained by NMR diffusion.

Sample	d_1 (μm)	d_2 (μm)	τ
Modern pine	16.0 ± 1.0	5.4 ± 0.6	7.0 ± 1.1
Archaeological pine	18.4 ± 3.5	13.6 ± 1.2	3.5 ± 0.6

having thick cell walls. Further information can be deduced from the tortuosity τ (Table 3). The modern pine shows a higher tortuosity (7.0 ± 1.1) compared to the archaeological pine (3.5 ± 0.6). However, for the ancient pine the normalized D data did not reach a limit value (see Figure 4). Therefore, we likely underestimated the value of tortuosity. Nevertheless, the tortuosity value obtained for modern pine seems to be in agreement with the literature value around 10 calculated for thermally modified *Pinus sylvestris* , also considering the effect of thermal modification and that we used a different species (*Pinus pinea*) [61]. Moreover, tortuosity is also in good agreement with the diffusion coefficient and diameters results. In fact, the higher the tortuosity, the more complicated the water routes. This means that the modern wood has a complex structure within which water cannot move easily. Conversely, the ancient pine has lost this complexity because of the structure's degradation, which has produced new voids and widened the existing pores lumens making the water motion easier. Specifically, the two different tortuosity values corroborate the pore size results obtained by NMR diffusion. Indeed, the low tortuosity measured for the ancient pine is compatible with its larger and more interconnected pores.

Differences in the pore size of the modern and the ancient pine were also found by using the low-field portable NMR, in good agreement with the high-field results. Specifically, in Figure 5a) the T_2 time distribution obtained by using the portable NMR is displayed and indicates that the archaeological pine (solid line) has longer T_2 than the modern pine (dashed line). The only exception is the shortest component around 1 ms that is longer for the modern wood than for the archaeological one. Since in previous works [62], [63] a component around 1 ms was attributed to bound water in the cell walls, we can suggest that bound water of the archaeological pine is highly influenced by paramagnetic impurities, whose accumulation is greater in more degraded areas, i.e. in the cell walls. This is confirmed by other studies [23], [64], where the T_2 component around 1 ms ascribable to bound water in the cell walls was not detected due to their strong degradation state. Since the T_2 is proportional to the degree of decay, we can suggest that the increment of T_2 for the ancient pine is a consequence of decay. This also means that water in the archaeological pine is located in larger structures and the water content has raised as shown by the probability associated with T_2 (Figure 5a). The pores diameter calculated from high-field diffusion-NMR (Table 3) can be compared with the pores diameter obtained by low-field T_2 distribution (Figure 5b). However, compared to high-field diffusion, the low-field relaxation measurements allowed to provide a global pore distribution of the sample while the intrinsic resolution of the diffusion-NMR is limited by the T_1. In our case, the maximum distance (ℓ_D) accessible is 43 μm [65] at $\Delta = 400$ ms and $D = 2.3 \times 10^{-9}$ m^2/s (the free water diffusion coefficient). Nevertheless, we think that in case of the archaeological pine the D vs Δ^{-1} behaviour is still affected by the presence of free-like water due to the existence of very large pores, not detectable with diffusion NMR techniques [54]. This explains why the archaeological pine shows pore distribution around 70 μm (Figure 5b) that was not detected by NMR diffusion. The pore size distribution displayed in Figure 5b) confirms the enlargement of pores in the archaeological pine as predicted by diffusion and T_2 measurements. However, the peak around 70 μm is quite broad indicating a continuous distribution among peak with diameter from about 55 μm to 90 μm. The most intense peak for the ancient pine is around 17 μm. It should be noticed that both the diameters obtained from diffusion (Table 3) and associated with earlywood and latewood are included in the peak around 17 μm. This indicates a continuous distribution among earlywood and latewood tracheids, likely with water exchange. For modern wood, the two predominant peaks as well as their probability in Figure 5b) are in good agreement with the diameters calculated from diffusion analyses, with the MR images and with the literature values [61], [66] in which the mean lumen diameter was found around 15 μm – 20 μm. The existence of two separate peaks shows distinct spins populations for earlywood and latewood.

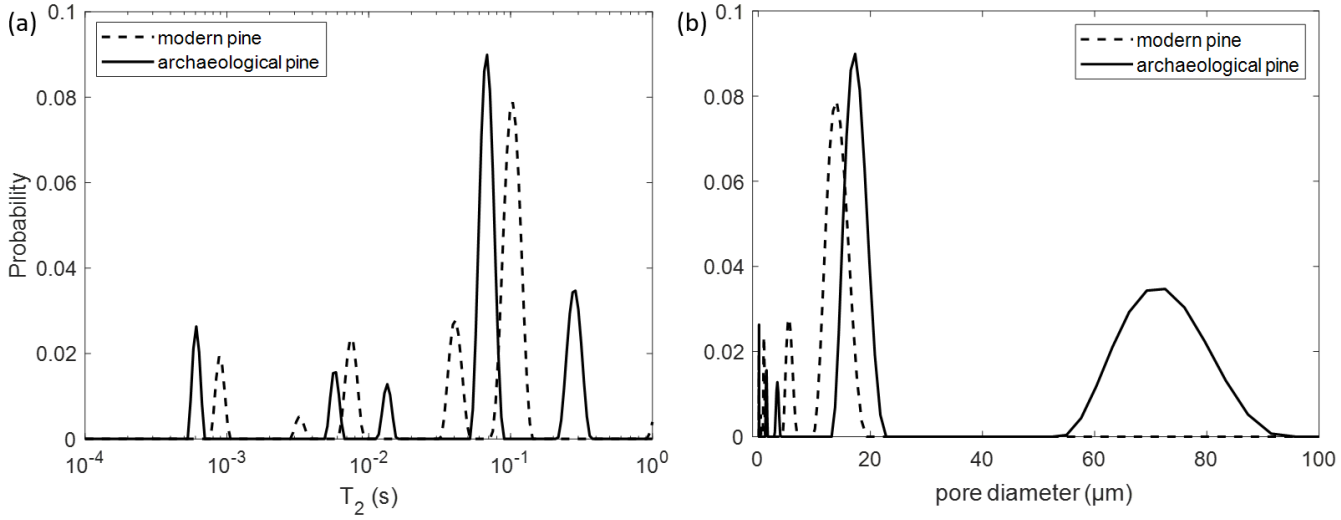

Figure 5. T_2 relaxation time distribution (a) and pore diameter distribution (b) for the modern pine (dashed line) and the ancient pine (solid line) obtained by using portable low-field NMR.

Smaller pore sizes can be associated to parenchyma cells and voids of the cell walls. Also in this case, the values obtained by equation (6) and displayed in Figure 5b) confirm that the ancient pine has larger pores (from 0.1 μm to 3 μm) than the modern pine (from 0.1 to 1 μm).

Particularly, the increment of size of the cell walls voids reveals the degradation of polymers constituting the cell wall itself.

6. CONCLUSION

This work suggests that by using high-field micro-MRI and high-field diffusion-NMR it is possible to obtain information about the archaeological wood decay. Information related to changes in the mean pore size, caused by wood decay, can be also obtained by low-field NMR relaxometry. The use of different NMR techniques and instrumentations provided the same result about the increment of the mean pore size for the archaeological pine wood. By comparing the modern pine sample and the ancient pine sample, the effect of the degradation process on the wood microstructure can be observed through the contrast of the MR images and quantified by the diffusion coefficient of water, the tortuosity and the pore size. The high-field NMR showed that the decay in pine wood mostly occurred in areas with high concentration of polymers, such as rays and latewood cell walls, with the enlargement of the pores lumen and the loss of wood structural complexity. MRI can also reveal morphological aspects of wood that are not observable with the naked eye, such as the annual rings, which can inform about past climate changes. In the pore size determination obtained by using portable low-field NMR, the method based on the T_2-distribution seems to be superior to the high-field diffusion method, whose resolution is limited by T_1. In conclusion, high-field techniques require a sampling; however, compared to other conventional analyses, they are non-destructive towards the sample that can be relocated in its original position in the artwork. The low-field portable NMR, instead, is mobile and suitable for in-situ analysis on samples of any size thus being non-invasive and non-destructive. Compared to high-field NMR it is also low cost, with shorter acquisition and processing time. We suggest that single-sided portable NMR is a powerful technique for revealing porosity changes of the entire wood structure produced by decay.

ACKNOWLEDGEMENT

The authors would like to thank the "Istituto Centrale per il Restauro" (ICR) of Rome (Italy) for providing the archaeological wood sample.

We acknowledge funding of Regione Lazio under the ADAMO project No. B86C18001220002 of the Centre of Excellence at the Technological District for Cultural Heritage of Lazio (DTC).

REFERENCES

[1] English Heritage, Waterlogged wood guidelines on the recording, sampling, conservation and curation of waterlogged wood, English Heritage Publishing, 2010, Product Code 51578.

[2] IAWA Committee, IAWA list of microscopic features for softwood identification, IAWA J. 25 (2004) pp. 1-70. DOI:1163/22941932-90000349

[3] Climate Data Information. Online [Accessed 15 March 2022] http://www.climatedata.info/proxies/tree-rings

[4] D. Castagneri, G. Battipaglia, G. von Arx, A. Pacheco, M. Carrer, Tree-ring anatomy and carbon isotope ratio show both direct and legacy effects of climate on bimodal xylem formation in Pinus pinea, Tree Physiol. 00 (2018) pp. 1-12. DOI: 10.1093/treephys/tpy036

[5] N. Macchioni, Wood: conservation and preservation. In: Smith C. (eds) Encyclopedia of Global Archaeology, Springer New York, 2014, ISBN 978-1-4419-0426-3. DOI: 10.1007/978-1-4419-0465-2_480

[6] D. H. Jennings, G. Lysek, Fungal biology: understanding the fungal lifestyle, BIOS Scientific Publishers, Guildford, 1996, ISBN 978-1859961087.

[7] M. A. Jones, M. H. Rule, Preserving the wreck of the Mary Rose, In P. Hoffman (Ed.), Proc. of the 4th ICOM-Group on Wet Organic Archaeological Materials Conference, Bremerhaven, 1991, pp.25-48.

[8] R. A. Eaton, M. D. Hale, Wood: decay, pests and protection, Chapman and Hall Ltd, London, 1993, ISBN 0412531208.

[9] R. A. Blanchette, A review of microbial deterioration found in archaeological wood from different environments, Int. Biodeterior. Biodegradation 46 (2000) pp. 189–204. DOI: 10.1016/S0964-8305(00)00077-9

[10] N. B. Pedersen, C. G. Björdal, P. Jensen, C. Felby, Bacterial degradation of archaeological wood in anoxic waterlogged environments. In: Stability of complex carbohydrate structures. Biofuel, foods, vaccines and shipwrecks. Ed. S. E. Harding, The Royal Society of Chemistry, Cambridge, 2013, ISBN 978-1-84973-563-6, pp. 160–187.

[11] D. M. Pearsall, Paleoethnobotany: a handbook of procedures, 3rd edition, Routledge, 2015, ISBN 9781611322996.

[12] T. Nilsson, R. Rowell, Historical wood-structure and properties, J. Cult. Herit. 13 (2012) pp. S5–S9. DOI: 10.1016/j.culher.2012.03.016

[13] D. J. Cole-Hamilton, B. Kaye, J. A. Chudek, G. Hunter, Nuclear magnetic resonance imaging of waterlogged wood, Stud. Conserv. 40 (1995) pp. 41-50. DOI: 10.2307/1506610

[14] S. Maunu, NMR studies of wood and wood products, Prog. Nucl. Magn. Reson. Spectrosc. 40 (2002) pp. 151–174. DOI: 10.1016/s0079-6565(01)00041-3

[15] M. Bardet, A. Pournou, NMR studies of fossilized wood, Annu. Rep. NMR Spectrosc. (2017) pp. 41–83. DOI: 10.1016/bs.arnmr.2016.07.002

[16] A. Salanti, L. Zoia, E. L. Tolppa, G. Giachi, M. Orlandi, Characterization of waterlogged wood by NMR and GPC techniques, Microchem. J. 95 (2010) pp. 345–352. DOI: 10.1016/j.microc.2010.02.009

[17] A. Maccotta, P. Fantazzini, C. Garavaglia, I. D. Donato, P. Perzia, M. Brai, F. Morreale, Preliminary 1H NMR study on archaeological waterlogged wood, Ann. Chim. 95 (2005) pp. 117–124. DOI: 10.1002/adic.200590013

[18] J. Kowalczuk, A. Rachocki, M. Broda, B. Mazela, G. A. Ormondroyd, J. Tritt-Goc, Conservation process of archaeological waterlogged wood studied by spectroscopy and gradient NMR methods, Wood. Sci. Technol. 53 (2019) pp. 1207–1222. DOI: 10.1007/s00226-019-01129-5

[19] M. Alesiani, F. Proietti, S. Capuani, M. Paci, M. Fioravanti, B. Maraviglia, 13C CPMAS NMR spectroscopic analysis applied to wood characterization, Appl. Magn. Reson. 29 (2005) pp. 177–184. DOI: 10.1007/bf03167005

[20] L. Rostom, D. Courtier-Murias, S. Rodts, S. Care, Investigation of the effect of aging on wood hygroscopicity by 2D 1H NMR relaxometry, Holzforschung 74 (2019) pp. 400-411. DOI: 10.1515/hf-2019-0052

[21] S. Viel, D. Capitani, N. Proietti, F. Ziarelli, A. L. Segre, NMR spectroscopy applied to the Cultural Heritage: a preliminary study

on ancient wood characterization, Appl. Phys. A 79 (2004) pp. 357–361.
DOI: 10.1007/s00339-004-2535-z

[22] V. Di Tullio, D. Capitani, A. Atrei, F. Benetti, G. Perra, F. Presciutti, N. Marchettini, Advanced NMR methodologies and micro-analytical techniques to investigate the stratigraphy and materials of 14th century Sienese wooden paintings, Microchem. J. 125 (2016) pp. 208–218.
DOI: 1016/j.microc.2015.11.036

[23] V. Stagno, S. Mailhiot, S. Capuani, G. Galotta, V.-V. Telkki, Testing 1D and 2D single-sided NMR on Roman age waterlogged woods, J. Cult. Herit. 50 (2021) pp. 95–105.
DOI: 10.1016/j.culher.2021.06.001

[24] D. Capitani, V. Di Tullio, N. Proietti, Nuclear magnetic resonance to characterize and monitor cultural heritage, Prog. Nucl. Magn. Reson. Spectrosc. 64 (2012) pp. 29–69.
DOI: 10.1016/j.pnmrs.2011.11.001

[25] C. Rehorn, B. Blümich, Cultural heritage studies with mobile NMR, Angew. Chem. Int. Ed. 57 (2018) pp. 7304–7312.
DOI: 1010.1002/anie.201713009

[26] P. T. Callaghan, Principles of nuclear magnetic resonance microscopy, Oxford University Press Inc, New York, 1991, ISBN 0-19-853944-4.

[27] W. S. Price, NMR studies of translational motion: principles and applications, Cambridge University Press, Cambridge, 2009, ISBN 978-0-521-80696-1.

[28] E. O. Stejskal, J. E. Tanner, Spin diffusion measurements: spin echoes in the presence of a time dependent field gradient, J. Chem. Phys. 42 (1965) pp. 288-292.
DOI: 10.1063/1.1695690

[29] P. N. Sen, Time-dependent diffusion coefficient as a probe of geometry, Concepts Magn. Reson. 23A (2004) pp. 1-21.
DOI: 10.1002/cmr.a.20017

[30] N. Proietti, D. Capitani, V. Di Tullio, Applications of nuclear magnetic resonance sensors to cultural heritage, Sensors 14 (2014) pp. 6977-6997.
DOI: 10.3390/s140406977

[31] D. Besghini, M. Mauri, R. Simonutti, Time-domain NMR in polymer science: from the laboratory to the industry, Appl. Sci. 9 (2019) pp. 1801.
DOI: 10.3390/app9091801

[32] D. G. Norris, The effects of microscopic tissue parameters on the diffusion weighted magnetic resonance imaging experiment, NMR Biomed. 14 (2001) pp. 77–93.
DOI: 10.1002/nbm.682

[33] D. A. Faux, P. J. McDonald, Nuclear-magnetic-resonance relaxation rates for fluid confined to closed, channel, or planar pores, Phy. Rev. E 98 (2018) pp. 1 – 14.
DOI: 10.1103/PhysRevE.98.063110

[34] A. V. Anisimov, N. Y. Sorokina, N. R. Dautova, Water diffusion in biological porous systems: a NMR approach, Magn. Reson. Imaging 16 (1998) pp. 565–568.
DOI: 10.1016/s0730-725x(98)00053-8

[35] R. Valiullin, V. Skirda, Time dependent self-diffusion coefficient of molecules in porous media, J. Chem. Phys. 114 (2001) pp. 452–458.
DOI: 10.1063/1.1328416

[36] F. A. L. Dullien, Porous media: fluid transport and pore structure, Academic Press, New York, 1991, ISBN: 9780323139335.

[37] P. P. Mitra, P. N. Sen, L. M. Schwartz, P. Ledoussal, Diffusion propagator as a probe of the structure of porous media, Phys. Rev. Lett. 68 (1992) pp. 3555–3558.
DOI: 10.1103/PhysRevLett.68.3555

[38] M. Zecca, S. J. Vogt, P. R. Connolly, E. F. May, M. L. Johns, NMR measurements of tortuosity in partially saturated porous media, Transp. Porous Media, 125 (2018) pp. 271-288.
DOI: 10.1007/s11242-018-1118-y

[39] K. R. Brownstein, C. E. Tarr, Spin-lattice relaxation in a system governed by diffusion, J. Magn. Reson. (1969) 26(1) (1977) pp. 17–24.
DOI: 10.1016/0022-2364(77)90230-X

[40] R. Kleinberg, M. Horsfield, Transverse relaxation processes in porous sedimentary rock. J. Magn. Reson. (1969) 88 (1990) pp. 9–19.
DOI: 10.1016/0022-2364(90)90104-H

[41] S. De Santis, M. Rebuzzi, G. Di Pietro, F. Fasano, B. Maraviglia, S. Capuani, In vitro and in vivo MR evaluation of internal gradient to assess trabecular bone density, Phys. Med. Biol. 55 (2010) pp. 5767.
DOI: 10.1088/0031-9155/55/19/010

[42] E. Toumelin, C. Torres-Verdín, B. Sun B, K. J. Dunn, Random-walk technique for simulating NMR measurements and 2D NMR maps of porous media with relaxing and permeable boundaries, J. Magn. Reson. 188 (2007) pp. 83–96.
DOI: 10.1016/j.jmr.2007.05.024

[43] M. Ronczka, M. Muller-Petke, Optimization of CPMG sequences to measure NMR transverse relaxation time T2 in borehole applications, Geosci. Instrum. Method. Data Syst. 1 (2012) pp. 197–208.
DOI: 10.5194/gi-1-197-2012

[44] H. Y. Carr, E. M. Purcell, Effects of diffusion on free precession in nuclear magnetic resonance experiments, Phys. Rev., 94 (1954) pp. 630–638.
DOI: 10.1103/PhysRev.94.630

[45] S. Meiboom, D. Gill, Modified spin-echo method for measuring nuclear relaxation times, Rev. Sci. Instrum. 29 (1958) pp. 688–691.
DOI: 10.1063/1.1716296

[46] X. Li, Z. Zhao, Time domain-NMR studies of average pore size of wood cell walls during drying and moisture adsorption, Wood Sci. Technol. 54 (2020), pp. 1241–1251.
DOI: 10.1007/s00226-020-01209-x

[47] P. R. J. Connolly, W. Yan, D. Zhang, M. Mahmoud, M. Verrall, M. Lebedev, S. Iglauer, P. J. Metaxas, E. F. May, M. L. Johns, Simulation and experimental measurements of internal magnetic field gradients and NMR transverse relaxation times (T2) in sandstone rocks, J. Petrol. Sci. Eng. 175 (2019) pp. 985–997.
DOI: 10.1016/j.petrol.2019.01.036

[48] G. H. Sørland, K. Djurhuus, H. C. Widerøe, J. R. Lien, A. Skauge, Absolute pore size distributions from NMR, Diffus. Fundam. 5 (2007) pp. 4.1-4.15.

[49] V. Di Donato, M. R. Ruello, V. Liuzza, V. Carsana, D. Giampaola, M. A. Di Vito, C. Morhange, A. Cinque, E. Russo Ermolli, Development and decline of the ancient harbor of Neapolis, Geoarchaeology 33 (2018), pp. 542–557.
DOI: 10.1002/gea.21673

[50] D. Giampaola, V. Carsana, G. Boetto, F. Crema, C. Florio, D. Panza, M. Bartolini, C. Capretti, G. Galotta, G. Giachi, N. Macchioni, M. P. Nugari, M. Bartolini, La scoperta del porto di "Neapolis": dalla ricostruzione topografica allo scavo e al recupero dei relitti, in Archaeologia maritima mediterranea: International Journal on Underwater Archaeology, Istituti editoriali e poligrafici internazionali, Fabrizio Serra, Pisa-Roma, 2005, pp. 1000–1045. [in Italian]. Online [Accessed 14 March 2022]
http://digital.casalini.it/10.1400/52974

[51] InsideWood.2004-onwards. Online [Accessed 13 March 2022].
https://insidewood.lib.ncsu.edu/

[52] Wood anatomy of central European species. Online [Accessed 13 March 2022].
http://www.woodanatomy.ch

[53] V. Stagno, C. Genova, N. Zoratto, G. Favero, S. Capuani, Single-Sided Portable NMR Investigation to Assess and Monitor Cleaning Action of PVA-Borax Hydrogel in Travertine and Lecce Stone, Molecules 26 (2021) pp. 3697.
DOI: 10.3390/molecules26123697

[54] V. Stagno, F. Egizi, F. Corticelli, V. Morandi, F. Valle, G. Costantini, S. Longo, S. Capuani, Microstructural features assessment of different waterlogged wood species by NMR diffusion validated with complementary techniques, Magn. Reson. Imaging 83 (2021), pp. 139-151.
DOI: 10.1016/j.mri.2021.08.010

[55] L. Venkataramanan, Y.-Q. Song, M. D. Hürlimann, Solving Fredholm integrals of the first kind with tensor product structure in 2 and 2.5 dimensions, IEEE Trans. Signal Process. 50 (2002) pp. 1017-1026.
DOI: 10.1109/78.995059

[56] P. M. Kekkonen, V.-V. Telkki, J. Jokisaari, Determining the highly anisotropic cell structures of pinus sylvestris in three orthogonal directions by PGSTE NMR of absorbed water and methane, J. Phys. Chem. B 113 (2009) pp. 1080.
DOI: 10.1021/jp807848d

[57] G. T. Tsoumis, Wood, Encyclopædia Britannica. Online [Accessed 14 March 2022]
https://www.britannica.com/science/wood-plant-tissue

[58] S. Takahashi, T. Kim, T. Murakami, A. Okada, M. Hori, Y. Narumi, H. Nakamura, Influence of paramagnetic contrast on single-shot MRCP image quality, Abdom. Imaging 25 (2000) pp. 511–513.
DOI: 10.1007/s002610000083

[59] A. Yilmaz, M. Yurdakoç, B. Işik, Influence of transition metal ions on NMR proton T1 relaxation times of serum, blood, and red cells, Biol. Trace Elem. Res. 67 (1999) pp. 187–193.
DOI: 10.1007/BF02784073

[60] S. Capuani, V. Stagno, M. Missori, L. Sadori, S. Longo, High-resolution multiparametric MRI of contemporary and waterlogged archaeological wood, Magn. Reson. Chem. 58 (2020) pp. 860-869.
DOI: 10.1002/mrc.5034

[61] M. Urbańczyk, Y. Kharbanda, O. Mankinen, V.-V. Telkki, Accelerating Restricted Diffusion NMR Studies with Time-Resolvedand Ultrafast Methods, Anal. Chem. 92 (2020) pp. 9948-9955.
DOI: 10.1021/acs.analchem.0c01523

[62] V.-V. Telkki, M. Yliniemi, J. Jokisaari, Moisture in softwoods: fiber saturation point, hydroxyl site content and the amount of micropores determined from NMR relaxation time distributions. Holzforschung 67 (2013) pp. 291–300.
DOI: 10.1515/hf-2012-0057

[63] P. M. Kekkonen, A. Ylisassi, V.-V. Telkki, Absorption of water in thermally modified pine wood as studied by nuclear magnetic resonance, J. Phys. Chem. C 118 (2014) pp. 2146–2153.
DOI: 10.1021/jp411199r

[64] S. Hiltunen, A. Mankinen, M. A. Javed, S. Ahola, M. Venäläinen, V.-V. Telkki, Characterization of the decay process of scots pine wood caused by Coniophora Puteana using NMR and MRI, Holzforschung 74 (2020) pp.1021–1032.
DOI: 10.1515/hf-2019-0246

[65] K. R. Brownstein, C. E. Tarr, Importance of classical diffusion NMR studies of water in biological cells, Phys. Rev. A, 6 (1979) pp. 2446–2453.
DOI: 10.1103/PhysRevA.19.2446

[66] I. Sable, U. Grinfelds, A. Jansons, L. Vikele, I. Irbe, A. Verovkins, A. Treimanis, Comparison of the properties of wood and pulp fibers from lodgepole pine (Pinus contorta) and scots pine (Pinus sylvestris), Bioresources 7 (2012) pp. 1771-1783.
DOI: 10.15376/biores.7.2.1771-1783